Aquat.sci.61 (1999) 260–278
1015-1621/99/030260-19 $ 1.50+0.20/0

Aquatic Sciences

Steady convective exchange flows down slopes

Jeff J. Sturman, Carolyn E. Oldham* and Greg N. Ivey

Centre for Water Research and Department of Environmental Engineering, University of Western Australia, Nedlands, Western Australia, 6907, Australia, e-mail: oldham@cwr.uwa.edu.au

Key words: Hydrodynamics, limnology, destabilising, convection, slopes, pollutants.

ABSTRACT

Horizontal exchange flows driven by destabilising buoyancy fluxes through the surface waters of lakes and coastal regions of oceans are important in understanding the transport of nutrients, micro-organisms and pollutants from littoral to pelagic zones. Our interest here is in the discharge flow driven by cooling or destabilising forcing at the water surface in a water body with variable depth due to sloping bottom topography. Flow visualisation studies and measurements in a laboratory model enabled us to develop scaling arguments to predict the dependency of discharge upon surface forcing and the angle of bottom slope. The results were used to interpret both the laboratory measurements and field data from a small shallow lake with sloping sides and an essentially flat bottomed interior, as well as published results from the literature. The steady state horizontal exchange can be described by $Q = 0.24\, B^{1/3}(l \tan\theta/(1 + \tan\theta))^{4/3}$, where Q is the discharge rate per unit length of shoreline, θ is the angle of the bottom slope, B is the surface buoyancy flux and l is the horizontal length of the forcing region over the slope. The flushing timescale of the wedge shaped littoral region was given by $\tau_f \sim l^{2/3}\,(1 + \tan\theta)^{4/3}/(B \tan\theta)^{1/3}$. While the buoyancy flux in the field is almost never constant in space or time and the slope from the shore is seldom uniform, we found that the exchange rate was relatively insensitive to buoyancy flux changes and only moderately sensitive to slope.

1. Introduction

This work is motivated by an interest in convectively driven horizontal exchange flows in the side-arms and shallow littoral regions of lakes, semi-enclosed seas and coastal ocean environments. Such flows are driven by spatial and temporal variation of buoyancy fluxes through the water surface and are affected by sloping bottom topography. We deal mainly with the steady state condition, although unsteady forcing can be an important feature of the field situation (e.g., Farrow and Patterson, 1993; Horsch et al., 1994; Sturman and Ivey, 1998).

Exchange flows in side-arms have been modelled using a variety of topographical assumptions and forcing arrangements. Early modelling of convectively driven

* Author for correspondence.

geophysical flows was undertaken in rectangular tanks with forcing on the vertical end walls (e.g., Cormack et al., 1974; Patterson and Imberger, 1980) generating important insights into the physical scaling of such flows. Yet in the field forcing fluxes are applied to the horizontal surfaces of the water, overlying bottoms which slope towards the deep water. Interest in flows down such slopes is often related to finding the rates of exchange of nutrients and pollutants from shallow to deep interior waters in lakes. Similarly, there is considerable interest in the transport of nutrients and pollutants from the bottom sediments of the lake to both the hypolimnic waters and higher up into the water column. For example, MacIntyre and Melack (1995) examined a range of physical processes for vertical and horizontal transport in lakes from their own measurements and the data of others. They developed a diagram of space and time scales of physical processes in Lake Biwa, Japan, and considered the geochemical and biological processes that might occur at these scales.

Considerable insight into these flows has been obtained from laboratory experiments with horizontally applied forcing over a sloping bottom (Horsch and Stefan, 1988a,b), in the field in sidearms of reservoirs (Monismith et al., 1990; James and Barko, 1991), and by using numerical modelling (Horsch and Stefan, 1988a,b; Horsch et al., 1994, unsteady flow) and both numerical and analytical techniques (Farrow and Patterson, 1993, with laminar unsteady flow). Flow visualisation studies of Horsch and Stefan (1988a,b) have helped to identify the mechanism which initiates the flow when the water surface is cooled and descending cold thermals subsequently set up mean flows down the bottom slopes. This destabilising mode of the surface forcing fluxes has been shown by Sturman and Ivey (1997) (SI hereafter) to be of considerable importance when compared with stabilising forcing.

The flow configuration studied experimentally by Horsch and Stefan (1988a,b) is shown diagrammatically in Figure 1, while the numerical studies (Horsch et al., 1994) were undertaken in a similar domain, with a circular segment replacing the vertical straight line terminating the wedge in Figure 1, for angles of bottom slopes of approximately 5, 11 and 23 degrees. From their numerical results Horsch and Stefan (1988a,b) calculated values of discharge (with an angle of slope of 11 degrees) and inferred that $Q \propto B^{1/n}$, where $2 < n < 3$. They also showed that steady state is approached only in a mean sense.

These early studies still leave unanswered some fundamental questions of relevance to biologists and chemists as well as to physical limnologists: how is the mean

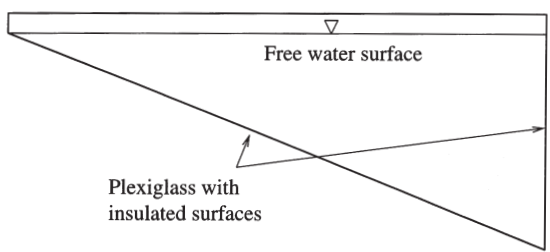

Figure 1. The experimental arrangement of Horsch and Stefan (1988a) in diagrammatic form. Cooling of the free water surface resulted in descending thermals which set up mean flows down the bottom slope. The angles of slope studied were approximately 5 and 11 degrees. Quasi steady state was achieved with this arrangement

or 'steady state' discharge down the slope dependent upon buoyancy flux and slope and when is it reached? The answers to both these questions are vital to estimate the net exchange of nutrients and chemicals between littoral and pelagic zones over the diurnal cycle. We address the above questions by undertaking both field and laboratory studies, while also drawing significantly from data in the literature. In Section 2 we describe field experiments in a shallow wetland, and present the results in Section 3. The laboratory methods we use are discussed in Section 4, while scaling arguments are developed in response to flow visualisation studies and in order to interpret our quantitative field and laboratory results. These results are combined and presented in Section 5 together with published data, while Section 6 contains our conclusions and final remarks.

2. Field methods

2.1. Rationale

Field measurements of convective circulation are scattered throughout the literature, often as additional data from studies focused on other processes. Preliminary investigations undertaken by the authors in shallow wetlands showed that identifiable daytime convective circulation occurred consistently whenever wind speeds dropped below 3 m s^{-1} simultaneous with periods of high insolation in the daytime and clear skies at night, giving rise to significant night-time cooling fluxes. Shallow wetlands offer an excellent opportunity to study convective circulation because of their rapid responses to changing meteorological conditions and logistically such measurements are relatively simple in wetlands compared with oceanic or large lake sidearms.

Therefore a short intensive field experiment was conducted by the authors in a small wetland in the Southern spring, when wind patterns were predictable, daytime insolation was very high and clear nights were frequent. Our preliminary data had shown that convective circulation was persistent during this season.

2.2. Site description

Lake Yangebup (32°6′40″S, 115°E) is in a region with a Mediterranean climate, has approximately 6.84×10^5 m^2 open water (Davis et al., 1993), an average depth of 2.5 m and a maximum depth of 3 m. Its topography is saucer like, with relatively steeply sloping sides and an essentially flat bottom over the interior. Bathymetric data indicates that the wetland bottom boundary slopes at an angle of approximately 1 degree.

2.3. Instrumentation

Given that vertical and horizontal stratification is a precursor for any convective exchange, two thermistor chains were deployed in the wetland. Site A was situated

in the centre of the wetland and was 3 m deep; Site B was on the edge of the wetland with a depth of 1.8 m. At each of these stations the chain consisted of five thermistors evenly spaced over the depth of the water column. Thermistors at Site A were located at 1.1 m, 1.6 m, 2.05 m, 2.4 m and 2.8 m water depths. Thermistors at Site B were located at 0.3 m, 0.6 m, 0.9 m, 1.2 m and 1.5 m.

Wind speed, wind direction and solar radiation sensors were also deployed at Site A. All sensors on both Sites A and B were logged every 20 min on a DATATAKER™ DT-500 data logger which was down-loaded every day during the intensive field experiment, which was carried out over a period of 4 days. Note that where times are mentioned they follow the 24 h convention rather than using am. or pm.

Velocity profiles were measured at both Sites A and B using a SONTEK™ 3D acoustic doppler velocity (ADV) probe. The significant readings were anticipated to be at Site B due to convergence near the centre of the lake (Site A) diminishing horizontal velocity components and enhancing vertical velocity components. At designated depths, the probe was clamped to a stainless steel pole driven into the sediments while data was collected for 60 s at 5 Hz. The clamp was then released, the probe lowered a further 0.5 m, clamped again and the next velocity timeseries was collected. This arrangement prevented spurious velocity fluctuations caused by the rocking of the boat from which we worked. We always completed such velocity 'profiles' within 20 min. ADV profile data was collected at 0.5 m, 1.0 m, 1.5 m, 2.0 m, 2.5 m and 2.8 m at the deep site. Profiles were performed at 10:30. At the shallow site, data was collected at 0.15 m, 0.5 m, 1.0 m and 1.8 m depths and at 9:30, 12:30.

3. Field results

As in our preliminary field investigations, evidence of convective circulation was obvious from thermistor chain data collected during the intensive field experiment, starting from midnight September 3rd 1996 (day 247). Figure 2a shows that wind speeds during this period were rarely above 4 m s^{-1}. Figure 2b shows heat fluxes into the lake peaked at 800 W m^{-2} at 14:00 of day 248, while destabilising heat fluxes out of the lake were approximately uniform over the three days at 200 W m^{-2} between 18:00 and 7:00.

Figure 3a shows the thermistor chain's data from shallow Site B, with the water column isothermal from 18:00, September 3rd (day 247) until around 10:00 September 4th (day 248) when surface heating began. The fingerprint of stabilising convective circulation appeared soon after 10:00 when data shows that simultaneous to surface water heating, bottom waters were cooling. The only possible mechanism for this is that while cooler water resulting from previous convective cooling is slowly circulated into the deeper parts of the wetland, surface waters are heated by current meteorological conditions. The opposite process would not typically be observed i.e., while warmer water created by previous surface heating is circulated out of the shallows, active convective cooling will rapidly mix that surface water through the water column, therefore destroying any obvious signature.

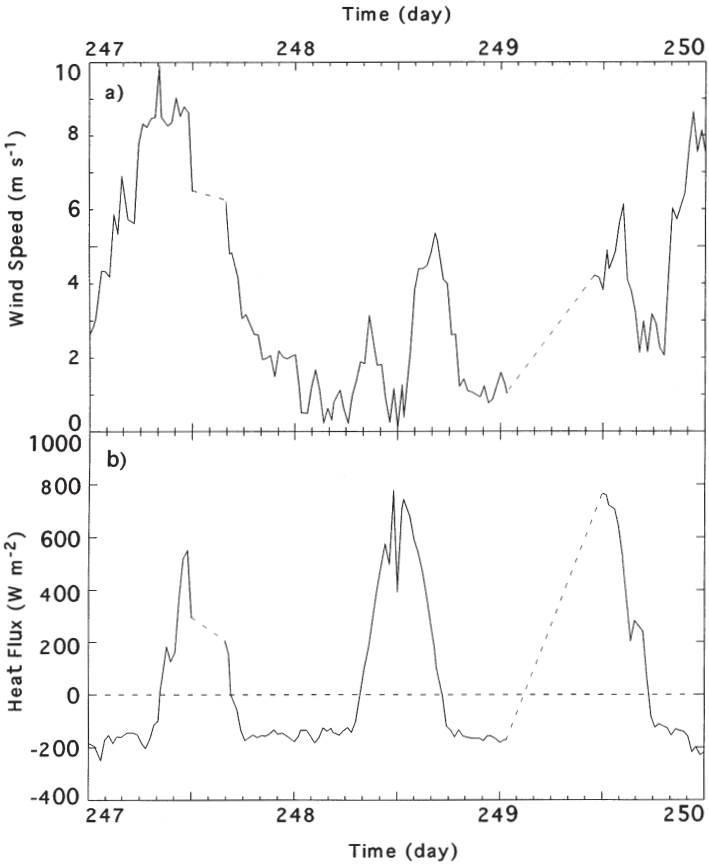

Figure 2. (a) Wind speeds measured at the centre of Lake Yangebup from September 3rd 1996 (day 247) to midnight September 5th 1996 (day 249). During the intensive field experiment on days 248 and 249, winds remained weak with peaks only of 5 m s^{-1}. (b) Heat fluxes into Lake Yangebup over the three day experiment. Night-time cooling fluxes remained constant over the three days at –200 W m^{-2}. Day time heating fluxes peaked at 800 W m^{-2} around 13:00 on days 248 and 249

Figure 3b shows the thermistor chain data from deeper Site A. It is qualitatively similar to that from Site B except the heating and cooling cycles are less differentiated, as would be expected at a deeper site. For example the slight temperature stratification observed at the shallow site from 10:00 to 18:00 of day 247 was not observed at Site A. Also the maximum temperatures measured at the deeper site (Fig. 3b) were 3 °C cooler than measured at the shallow site (Fig. 3a).

Figures 4a–c show the transition in velocity profiles observed on September 4th (day 248) at the shallow Site B. Convective circulation was detected initially at 9:50 as small bottom velocities opposite in direction to those measured in the surface layer. This is 16 h after the start of a destabilising forcing flux (see Fig. 2b) and is broadly consistent with Farrow and Patterson's (1993) finding that the lag in the response to the forcing flux could be up to 12 h. At 12:40, water velocities were

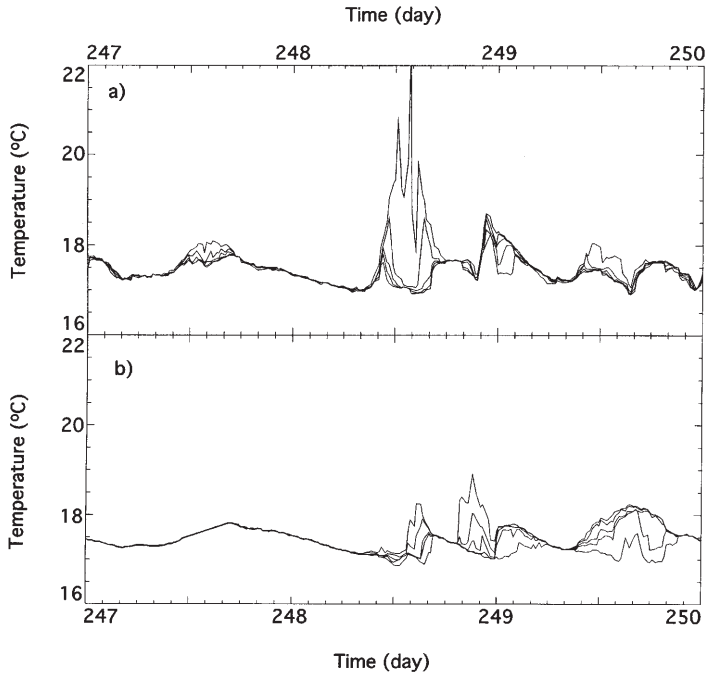

Figure 3. Thermistor chains data collected at (a) Site B and (b) Site A. Thermistors at the shallow Site B were located at 0.3 m, 0.6 m, 0.9 m, 1.2 m and 1.5 m water depth. Thermistors at the deep Site A were located at 1.1 m, 1.6 m, 2.05 m, 2.4 m and 2.8 m water depth

constant with depth. By 17:10, a reversal of velocities was again observed between surface and bottom waters. Note from Figure 2a that the only time wind speeds were greater than 3 m s^{-1} was from 10:00 to 12:00, a probable explanation for the uniform velocities observed in Figure 4b. Similar velocity profiles are used later in the paper for comparison with scaling arguments.

Several major points emerge from the field data. First, there are indeed significant flows associated with the thermal forcing through the water surface in the absense of substantial winds. Second, the flows are not in phase with the surface forcing and particularly the direction of the flows is not in phase with that expected from the sign of the forcing; we see phase lags between the forcing and the responses in general. Third, we see spatial variations in the lag when comparing responses at A and B. These issues mean it is not easy to interpret the temperature and velocity data without knowledge of the timescale required to establish a flow driven by destabilising convective forcing and the spatial form of the flow.

4. Laboratory methods

In response to the complexities of the data from field measurements, we undertook laboratory studies with a view to clarifying the spatial form of the flow and under-

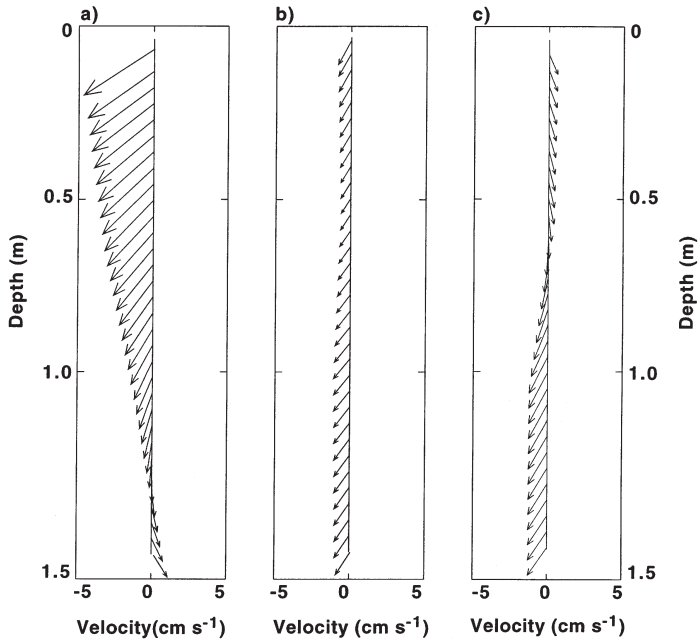

Figure 4. Velocity profiles collected at the shallow Site B at (a) 9:50 (b) 12:40 and (c) 17:10 on day 248. Positive horizontal components of the velocity indicate downslope flow, i.e., flow away from the shore. Profiles at 9:50 and 17:10 show a reversal of velocities from top to bottom waters, which, when coincident with low wind speeds, is considered indicative of convective circulation

standing better the flow dynamics. We used a laboratory facility described in detail in SI and diagrammatically represented in Figure 5. This facility enabled us to control the boundary conditions of the flow accurately and to extend our discharge data orders of magnitude below those found in the field. The facility consisted of a rectangular perspex box of dimensions 2000 mm long, 500 mm wide and 100 mm high, insulated with at least 50 mm of polystyrene foam. Horizontal copper plates extended from each end of the tank 250 mm into the interior at the top of one end and at the bottom of the other end, covering the full width of the tank. These plates constituted the front walls of two heat exchangers through which heated water could be circulated at one end of the tank while chilled water was circulated at the other end, thus yielding symmetrical forcing fluxes of opposite signs on the horizontal surfaces at the tank ends. The mean tank temperature was thereby maintained at a constant value essentially equal to the laboratory air temperature, thus minimising heat losses which amounted to only about 1% of the heat flux through the tank (see SI).

In the present study, the topography of the ends was changed by fitting perspex slopes opposite to the forcing plates, with zero depth at the tank end wall and 100 mm depth at the edge of the forcing region, resulting in a slope angle of 22 deg. A destabilising buoyancy flux of approximately $B \cong 3.5 \times 10^{-8}$ m^2 s^{-3} was applied at each forcing region, with a starting e-folding timescale of approximately 23 s (see SI for a plot showing the form of time development of B). Note that the present ar-

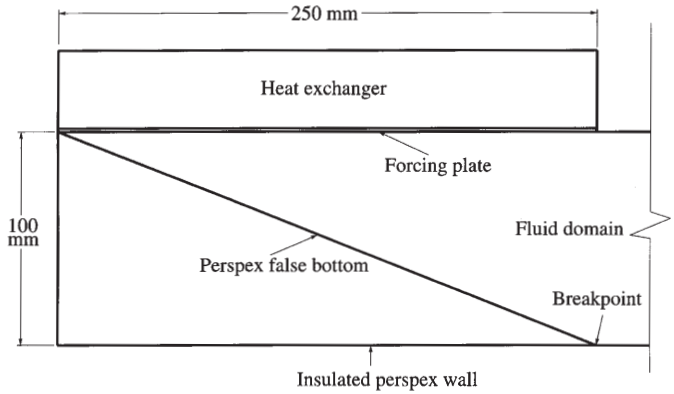

Figure 5. The experimental arrangement in this work for flow visualisation studies and velocity measurements using a *p*article *i*mage *v*elocimetry method (PIV). The figure shows one end only of a two ended experiment, with cooling at the end shown and heating at the bottom of the other end

rangement differs from that of Horsch et al. (1994) as the heat flux over our horizontal boundary was not applied in a free slip manner.

For both flow visualisation and velocity measurements the water in the tank was seeded with fluorescent particles ranging in size from 45 to 120 μm and illuminated near the tank centre by a vertically oriented sheet of laser light from an argon ion laser. A particle image velocimetry (PIV hereafter) method was used to measure velocities as detailed in Stevens and Coates (1994) and SI.

5. Laboratory results

5.1. Observations of the flow

We undertook flow visualisation studies in the region above the slope and extending a short distance into the interior of the tank. The forcing at this end of the tank is in the destabilising sense, that is the upper boundary is being cooled. Figures 6a–e are a series of images for a typical experiment captured from the video record of the flow taken from just after switching on the cooling above the slope and the anti-symmetric heating at the other end of the tank and extending through to steady state.

The thermal boundary layer has become unstable 26 s after switching on the cooling surface and, above the point labelled ‘A’ in Figure 6a, negatively buoyant thermals (dark) are visible descending from the forcing plate. In Figure 6b (60 s), a mean flow down the slope has been established and has emerged into the interior of the tank, with a front at ‘E’. A corresponding surface inflow along the upper wall is clearly evident. Below ‘F’ in Figure 6c (278 s) is a spectacular separation feature from the bottom boundary (see too Sturman et al. (1996) and SI, where a similar feature is seen with different geometries). This feature has been squeezed vertically by the arrival (Fig. 6d, 297 s) at ‘G’ of the forced flow from the other end of the tank caused by the heating plate at the bottom of that end. Thermals are evident

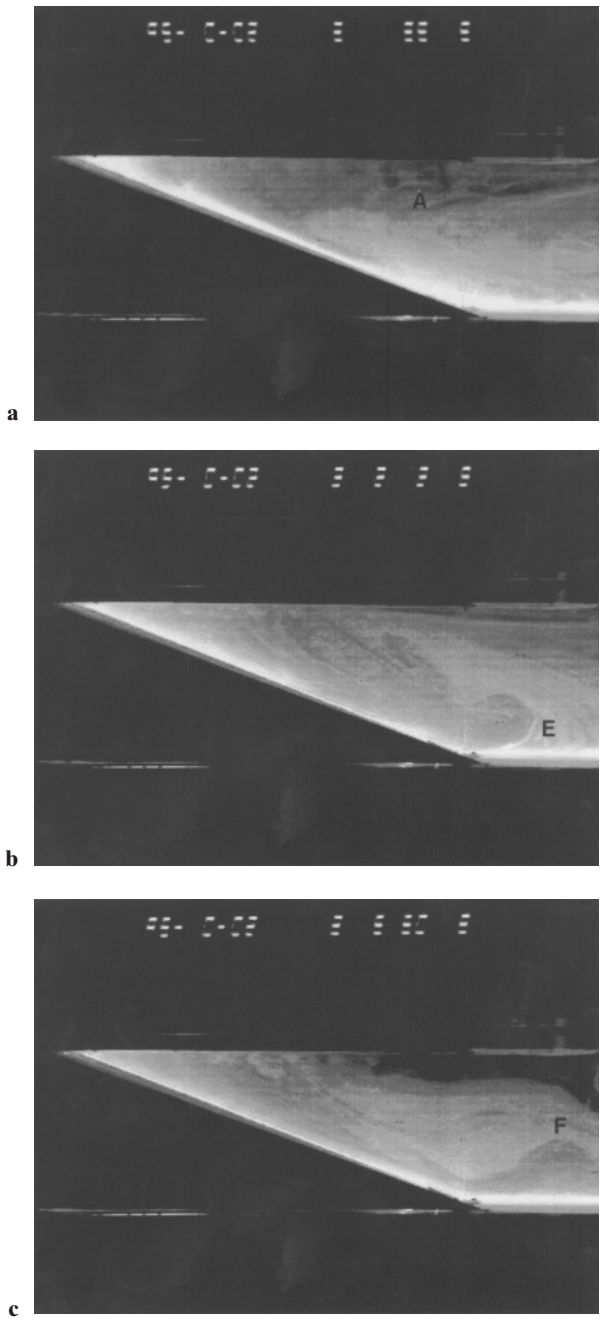

a

b

c

Figure 6a–c. A series of flow visualisation images from just after cooling had begun to approaching 'steady state'. (a) Thermals are just starting to descend above 'A' at 26 s after thermal start; (b) Mean flow is emerging from the sloping region, 'E' at 60 s after thermal start; (c) A feature of separated flow from the bottom boundary is visible below 'F' at 278 s

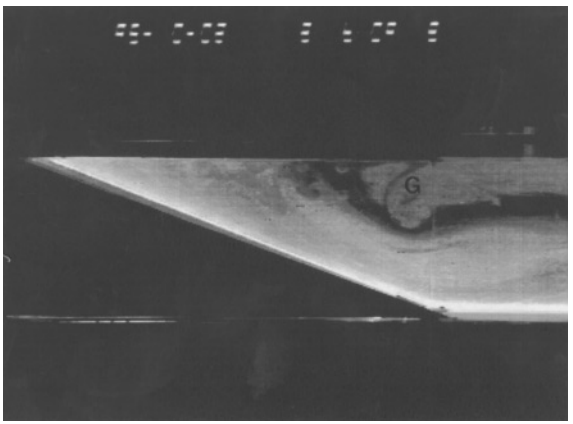

d

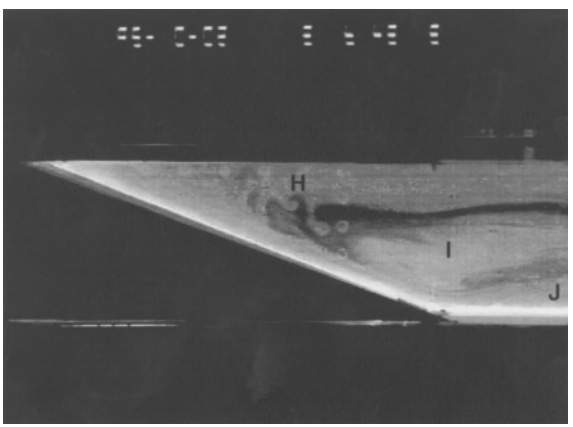

e

Figure 6d–e. (d) Flow deriving from the forcing at the other end of the tank is penetrating the wedge region at 'G' at 297 s; (e) This is visually representative of steady state at 331 s after thermal start

ahead of this incoming front and show the effects of horizontal shear. This is more clearly seen in Figure 6e (331s), where the sheared thermals are located beneath the label 'H' and this figure represents near steady state conditions. Note that the central region around 'I' appears quiescent and below it at 'J' the separation feature persists, although its subsequent shape and size vary with time.

In general these observations of flow down the slope are consistent with those reported by Horsch and Stefan (1988a,b) and Horsch et al. (1994). The region of separation from the bottom of the flow emerging from down the slope constitutes an additional feature (see for example Turner (1973) p.70 too, and, for a different geometries, Patterson and Armfield (1990) and Sturman et al. (1996)), which could influence the transport of nutrients and pollutants from bottom sediments.

The steady state flow shown in Figure 6e corresponds with the velocity vector map in Figure 7. The velocities were obtained with a PIV technique (see above), with intense velocities down-slope up to 18 mm s^{-1} in this example.

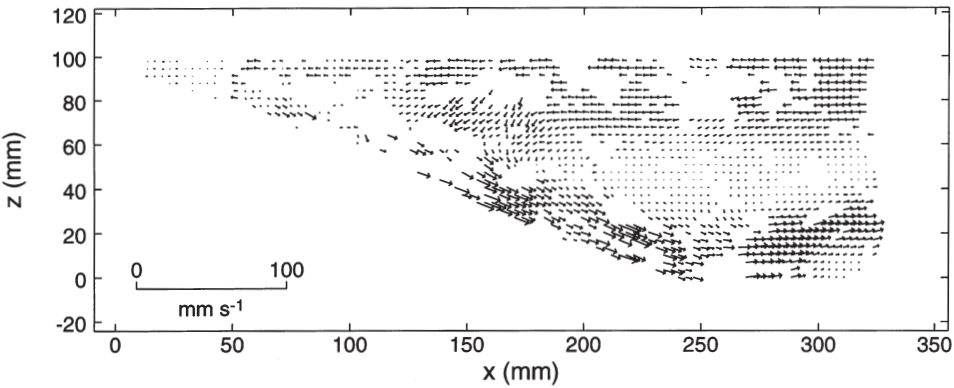

Figure 7. This velocity vector map corresponds with Figure 6e. It is derived from a particle image velocimetry (PIV) process and demonstrates intense flow down the slope with a maximum velocity of 18 mm s^{-1} in this case

5.2. Flow dynamics

5.2.1. Background

A background description of the earlier work of Sturman et al. (1996) will enable the reader to understand more easily the scaling analysis which follows. In that work the authors described a series of experiments in a rectangular tank, which had a portion of the bottom boundary heated by a plate at one end while a portion of the upper boundary was simultaneously cooled at the other end; thus at each end the forcing was applied in a destabilizing sense. The aspect ratio of the length of the forcing plate to the height of the tank (l/H) was one, an important point as will be seen below. Heating was turned on at one end of the tank while cooling was simultaneously turned on at the other end. Thermals formed and rose at the heated end (or sank at the cooled end) into the surrounding water, causing a horizontal temperature difference and thus a horizontal density difference between the regions adjacent to the forcing plates and the interior of the tank. Over time this resulted in a mean horizontal flow from the tank interior. A turbulent boundary layer dominated by rising thermals formed along the heated plate, with the mean horizontal flow discharging from the boundary layer towards the end wall where it was turned through 180 degrees and proceeded into the interior of the tank along the wall opposite to the forcing plate. Without reproducing the details of the scaling, we outline the broad line of the argument and the crucial results.

Sturman et al. (1996) selected the dominant terms of both the thermal energy equation and the momentum equation (horizontal and vertical components) within the turbulent boundary layer flow associated with the forcing plate and reduced them to algebraic equations by introducing appropriate scales for the variables. Within the thermal energy equation it was assumed that vertical turbulent diffusion of heat associated with the rising thermals (heated end) balanced horizontal convection. A pressure/turbulent stress balance was assumed for the horizontal com-

ponent of the momentum equation, with the dominant terms in the vertical component taken to imply a pressure/buoyancy balance. Eliminating the pressure terms between the two components of the momentum equation, introducing appropriate scales and solving the scaled thermal energy equation and the momentum balance gave rise to the following important results:

$$h \sim l \tag{1}$$

and

$$Q \sim uh \sim (Bl)^{1/3} h \tag{2}$$

where h (m) is the thickness of the turbulent boundary layer, l (m) is the length of the forcing plate, Q ($m^2 s^{-1}$) is the discharge per unit width, u ($m s^{-1}$) is the mean horizontal velocity scale of the boundary layer and the uniform buoyancy flux B ($m^2 s^{-3}$) through the surface of the water is given by,

$$B = g\alpha\tilde{H}/\rho_0 C_p, \tag{3}$$

where g ($m s^{-2}$) is the acceleration due to gravity, α (K^{-1}) is the coefficient of thermal expansion of water, $\tilde{H}$ ($W m^{-2}$) is the heat flux out through the water surface, ρ_0 ($kg m^{-3}$) is the surface water density and C_p ($J kg^{-1} K^{-1}$) is the specific heat of water.

Equation 1 means that the thickness of the turbulent boundary layer (dominated by the thermals moving away from the forcing surface) is of the same order of magnitude as the length of the forcing plate. In fact the coefficient of proportionality was approximately 0.5 (see Sturman et al., 1996) and thus the aspect ratio $l/H = 1$ implied that the boundary layer was unconstrained. This is a necessary condition for the scaling of eq. 1 to hold true and provides the foundation for us to use the above results in the scaling arguments for the new arrangement of this paper, i.e., a sloping bottom beneath a cooled region with destabilizing convection resulting in mean horizontal exchange flows.

5.2.2. Description of steady state wedge flow

In order to consider the flow associated with a cooled region above a sloping bottom, refer to Figure 8, which shows the definitions of axes and some major variables. From Figure 7 we see that there is an almost quiescent region which extends into the wedge a distance l_1 from the interior flow (from x = 250 mm to about x = 175 mm). Below it there is a strong flow down-slope, while above the quiescent region resides a turbulent boundary layer whose thickness scales as distance from the forcing plate edge at x = 250 mm (see Sturman et al. (1996)). This boundary layer is unconstrained until at x = 175 mm it meets the underflow, at which point the order of magnitude of its thickness is given from eq. 1 and the geometry by

$$h \sim l_1 \sim l \tan\theta/(1 + \tan\theta) \tag{4}$$

where l is the length of the forcing plate, θ is the angle of the slope and $h_g/\cos\theta$ has been neglected compared with H (see too Fig. 7) where h_g is the gravity current thickness normal to the slope.

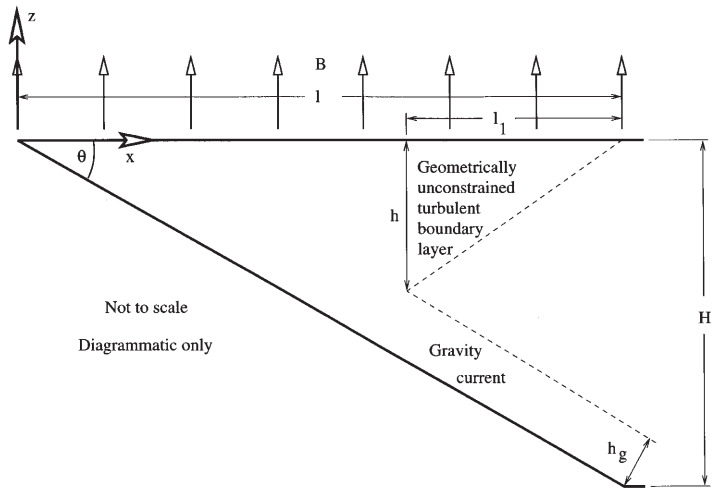

Figure 8. The definition of axes and major symbols in the sloping region. The description of the flow dynamics in §5 depends upon the definitions visually represented here

From Sturman et al. (1996) the discharge per unit width (i.e., the direction normal to the plane of Figs. 7 and 8) from the turbulent boundary layer below the forcing region at is given by:

$$Q \sim (Bl_1)^{1/3} h\,. \tag{5}$$

Notice that by continuity the discharge down the slope must be identical to that from the turbulent boundary layer at this point ($x = l - l_1$). This implies that the remainder of the forcing region (i.e., $0 < x < l - l_1$) contributes to an increase in the buoyancy anomaly of the fluid discharging into the gravity current but does not further increase the discharge itself. The discharge is obtained by substituting eq. 4 into eq. 5 to give:

$$Q \sim B^{1/3} (l \tan\theta/(1 + \tan\theta)^{4/3}. \tag{6}$$

Thus for small θ, i.e., $\tan\theta < 1$,

$$Q \sim B^{1/3}\, l^{4/3}\, \theta^{4/3}. \tag{7}$$

The steady state thermal energy balance in the control volume comprising the wedge requires that

$$Bl \sim Q g' \tag{8}$$

and by using eq. 6, the buoyancy anomaly of the gravity current leaving the wedge is given by:

$$g' \sim B^{2/3} ((1 + \tan\theta)/\tan\theta)^{4/3}/l^{1/3}. \tag{9}$$

Both the thickness of the gravity current and its velocity scale can be found from the momentum balance for the flow down the slope, yet whether the appropriate balance of terms is a turbulent friction/buoyancy balance or an inertia/buoyancy balance is not readily determined. With field application in mind, an upper bound to the thickness of the gravity current (and a lower bound for the velocity) will arise from assuming a turbulent friction/buoyancy balance, as the velocity will then attain a constant value rather than increasing without limit on the slope (Turner, 1973). From Turner (1973) the latter balance is:

$$C_D U^2 \sim g' h_g \sin\theta, \tag{10}$$

where C_D is a drag coefficient, U is a mean steady state velocity scale for the gravity current parallel to the slope, and h_g is the thickness. Also continuity requires

$$Q \sim U h_g . \tag{11}$$

Substitution of eq. 11 into eq. 10 and use of eqs. 8 and 9 results in the gravity current thickness scale

$$h_g \sim (C_D/\sin\theta)^{1/3}\{\tan\theta/(1+\tan\theta)\}^{4/3} l, \tag{12}$$

while the corresponding velocity follows from substituting eqs. 6 and 12 into 11 to give:

$$U \sim (Bl \sin\theta/C_D)^{1/3}. \tag{13}$$

5.2.3. Timescale

The flushing timescale, τ_f, is the timescale in which we are interested, being a measure of the time taken to flush the region above the slope; it is given by the volume of fluid above the slope divided by the discharge:

$$\tau_f \sim Hl/2Q \sim Hl/Q. \tag{14}$$

We obtain the flushing timescale by substituting from eq. 6 into 14:

$$\tau_f \sim l^{2/3}(1+\tan\theta)^{4/3}/(B\tan\theta)^{1/3}. \tag{15}$$

The 'filling-box' timescale is commonly used to measure attainment of steady state in laboratory cavity convection experiments (see Sturman et al., 1996 for example) and eq. 15 becomes identical to this timescale in water bodies appropriately modelled by wedges. This is the case for most lakes and sidearms in the field.

5.3. Discharge results

Values of the discharge from the sloping region to the interior of the laboratory experimental tank were derived from a series of three velocity vector maps like that shown in Figure 7. Of these, one was at the sloping region and two were at the

centre of the tank. The discharge was found from the velocity vector map of the sloping region by averaging vectors over 11 columns (about 35 mm) of each row just to the right-hand side of the 250 mm mark. The averaged rows gave a velocity profile in the z-direction, which was integrated from the horizontal boundary to the zero velocity cross-over point. An average was taken of the two resulting estimates of discharge and this was extended over the results from the three velocity maps. At the tank centre the rows were averaged over almost the whole of the range of x, otherwise the process was the same. The values of discharge per unit width are presented in figures 9 and 10, which will be discussed in detail in Section 6 below.

6. Discussion

We are now in a position both to test the description of the flow dynamics against data and to interpret data drawn from field, laboratory, and numerical experiments. Note that to maintain consistency in comparing results from Lake Yangebup with other field data and with the laboratory results, we have modelled the lake as a wedge.

The published literature contains data drawn from laboratory and numerical experiments and from the field (see §1) which, when used in conjunction with our own results, enable us to evaluate the scaling presented above. Field data in the literature are not always accompanied by detailed accounts of topographical variations of the bottom, or of variations in space and time of the forcing buoyancy fluxes. Thus the issue of the sensitivity of discharge to variations in both buoyancy flux and angle of slope is pertinent here. Equation 7 indicates that discharge is insensitive to changes in buoyancy flux (it depends on the 1/3 power of B), while the sensitivity of discharge to angle of slope at small angles is moderate (with a power of 4/3). We conclude that more care is warranted when estimating angles of slope in the field than is called for in estimating buoyancy flux.

As the flows set up in response to the thermal forcing are not in phase with the forcing (see above Section 3), the flow measured in the field will approximate steady state flow when it is measured at a time of the order of the flushing timescale (see Eq. 15) after the onset of the associated destabilising forcing. For example, in the case of Lake Yangebup destabilising forcing commences at 16:00 on day 247. The associated steady state flow response would be expected at $\tau_f \sim O(21)$ h later at 13:00 on day 248. The latest downslope discharge available on day 248 was at approximately 10:00 (see Fig. 4) i.e., 18 h after the onset of destabilising forcing and we accepted this discharge as close to the steady-state value. We similarly determined the approximate steady-state discharge values from the other field results.

The data we have drawn from the literature and from both our field and laboratory work is plotted with the scaled discharge on the abscissa and the experimental discharge (Q_{ex}) on the ordinate in Figure 9, covering three orders of magnitude of change in the discharge. The angles of slope represented in Figure 9 range over approximately $0.4 \leq \theta \leq 22$ degrees. The three experimental data points of Horsch and Stefan (1988a,b), derived from experiments where the boundary conditions were determined by the laboratory environment, were thus quasi-steady, yet carefully calibrated and well controlled compared with the field situation. Of the

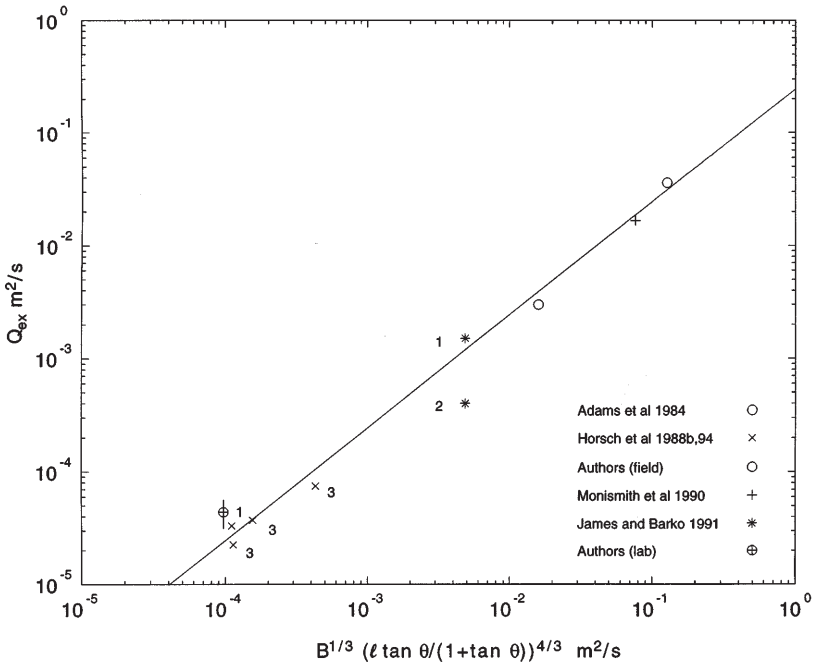

Figure 9. Dimensional numerical, field and laboratory experimental discharge (Q_{ex}) versus discharge predicted by the scaling of eq. 4. The points labelled '1' are numerical model results, '2' is a field experimental result with reeds present in the water while points labelled '3' are laboratory experimental discharges. The un-numbered points of Adams and Wells (1984) and Monismith et al. (1990) both derive from field experiments. The laboratory experimental result of the present work has an error bar representing ±1 standard deviation. The experimental values of discharge cover three orders of magnitude, agreeing very well with the scaling prediction. The equation for the line is $Q = 0.24\ B^{1/3}\ (l \tan\theta/(1 + \tan\theta))^{4/3}$, (eq. 16)

two points identified as 'James et al.' the lower is a field experimental discharge with reeds in the littoral zone, while the upper point is a numerical result derived from the model of Horsch and Stefan (1988a), with the boundary conditions of the model corresponding with those in the field. The large disparity between the points is hardly surprising, given the presence of the reeds in the field results. The points from Adams et al. (1984), Monismith et al. (1990) and our own field data are in remarkably good agreement with the scaling. Discharges from field data were corrected for variations in width, cross section and slope. The solid line in Figure 9 is the least squares best fit of eq. 6 to the data ($\varrho^2 = 0.98$ where ϱ is the correlation coefficient) and results in

$$Q = 0.24\ B^{1/3}\ (l \tan\theta/(1 + \tan\theta))^{4/3}. \qquad (16)$$

The data support the scaling very well over the range of discharges plotted.

Figure 10 shows the same data set plotted to demonstrate the effect of the slope. The point from the authors' laboratory experiments is for the largest angle represented. The point from James and Barko (1991) relating to the field datum with

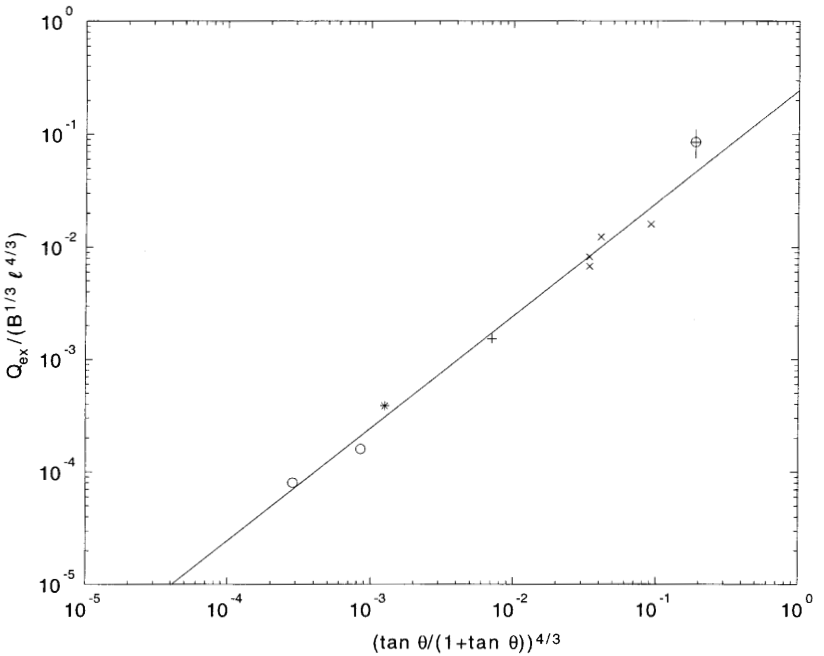

Figure 10. Non-dimensional discharge versus slope, with the range of angles of slope given by $0.4 \leq \theta \leq 22$ degrees. As in Figure 9 where the sources of the points are identified, there is very good agreement between the non-dimensional discharge and the scaling predictions over three orders of magnitude variation of the abscissa. The line derives from the same equation as in Figure 9 and eq. 16

reeds present has been left off Figure 10, as it is not directly relevant to our work. The solid line is the same as that fitted in Figure 9.

7. Conclusions

The results lead to the steady state discharge as described by eq. 16, which clearly shows only a weak, but essential, dependency on the measured buoyancy flux. Discharge is more sensitive to variations of angles of slope, particularly for small angles. The flushing timescale of the sloping region was derived (eq. 15). The result for discharge (eq. 16) receives strong support from laboratory experimental data and from field and numerical data ranging over three orders of magnitude variation of discharge.

Consider now some typical values of parameters for water bodies in the field. For Lake Yangebup (see §2) $l \sim 500$ m, $H \sim 3$ m, (so $\theta \sim 0.34$ deg), $B \sim 1 \times 10^{-7}$ m^2 s^{-3} and a typical field value of C_D is (see Turner, 1973) $C_D \sim O(10^{-3})$. Substituting these into eq. 12 gives $h_g \sim 0.3$ m, $U \sim 70$ mm s^{-1} (from eq. 13) and flushing timescale of $O(21)$ h (eq. 15). In this case it is not clear whether flushing of the lake and attainment of quasi-steady state can occur diurnally. Repeating the timescale calculations

for a typical small reservoir sidearm (e.g., Monismith et al., 1990) using the same buoyancy flux and $l \sim 500$ m, $H \sim 10$ m (to the diurnal thermocline) results in a flushing time of order 14 h. Thus we expect that the flushing of sidearms and near shore regions of wetlands might occur diurnally, consistent with the earlier conclusions of Farrow and Patterson (1993), for example, in their laminar flow model.

The significance of such convective circulation, and its effect on flushing of littoral zones, increases with increased sheltering of water bodies from prevailing winds. Such sheltering would decrease the frequency of wind-driven mixing and circulation and under such conditions it is frequently assumed that thermal stratification and possibly bottom water anoxia would result. This study has shown that a mechanism exists, under appropriate meteorological forcing, which may be effective in preventing such stratification. Knowledge of such processes has already been utilised by the authors in the design of pollution control wetlands. Due to public safety concerns these wetlands were extremely sheltered therefore the design was manipulated, using scaling developed in this paper, to optimise convective circulation during periods of minimal flow.

The results presented in this paper are thus readily applicable to studies of the exchange of nutrients and pollution between the littoral and pelagic zones of sheltered water bodies. However in many shallow water bodies, such zones are also encroached by submerged macrophytes. The effect of such vegetation on the convective circulation described here is the subject of continuing work by the authors.

ACKNOWLEDGEMENTS

The authors thank S. Bell who helped with field data collection and processing and D. Farrow, P. Jacobs and the anonymous reviewers who made useful comments on an earlier version of this paper. This work is funded by the Australian Research Council. Centre for Water Research Reference ED-1277-JJS.

REFERENCES

Adams, E.E. and S.A. Wells, 1984. Field measurements on side arms of Lake Anna, Va. J. Hydraul. Engg. 110: 773–793.

Cormack, D.E., L.G. Leal and J. Imberger, 1974. Natural convection in a shallow cavity with differentially heated end walls. J. Fluid Mech. 65: 209–229.

Davis, J.A., R.S. Rosich, J.S. Bradley, J.E.Growns, L.G. Schmidt and F. Cheal, 1993. Wetlands of the Swan Coastal Plain, Vol. 6: Wetland classification on the basis of water quality and invertebrate community data. Perth: Water Authority of Western Australia and Environmental Protection Agency.

Farrow, D.E. and J.C. Patterson, 1993. On the response of a reservoir sidearm to diurnal heating and cooling. J. Fluid Mech. 246: 143–161.

Horsch, G.M. and H.G. Stefan, 1988a. Convective circulation in littoral water due to surface cooling. Limnol. Oceanogr. 33: 1068–1083.

Horsch, G.M. and H.G. Stefan, 1988b. Cooling-induced convective littoral currents in lakes: simulation and analysis. Project report no. 272, University of Minnesota St. Anthony Falls Hydraulic Laboratory.

Horsch, G.M., H.G. Stefan and S. Gavali, 1994. Numerical simulation of cooling-induced convective currents on a littoral slope. Intern. J. Num. Methods Fluids 19: 105–134.

James, W.F. and J.W. Barko, 1991. Estimation of phosphorus exchange between littoral and pelagic zones during nighttime convective circulation. Limnol. Oceanogr. 36: 179–187.

MacIntyre, S. and J.M. Melack, 1995. Vertical and horizontal transport in lakes: linking littoral, benthic and pelagic habitats. J.N. Am. Benthol. Soc. 14: 599–615.
Monismith, S., J. Imberger and M.L. Morison, 1990. Convective motions in the sidearm of a small reservoir. Limnol. Oceanogr. 35: 1676–1702.
Patterson, J.C. and S.W. Armfield, 1990. Transient features of natural convection in a cavity. J. Fluid Mech. 219: 469–497.
Patterson, J.C. and J. Imberger, 1980. Unsteady natural convection in a rectangular cavity. J. Fluid Mech. 100: 65–86.
Stevens, C.S. and M.J. Coates, 1994. A maximised cross-correlation technique for resolving velocity fields in laboratory experiments, J. Hydr. Res. 32: 195–211.
Sturman, J.J., G.N. Ivey and J.R. Taylor, 1996. Convection in a long box driven by heating and cooling on the horizontal boundaries. J. Fluid Mech. 310: 61–87.
Sturman, J.J. and G.N. Ivey, 1998. Unsteady convective exchange flows in cavities. J. Fluid Mech. 368: 127–153.
Turner, J.S. 1973. Buoyancy effects in fluids. Cambridge University Press, Cambridge, 367 pp.

Received 6 February 1998;
revised manuscript accepted 1 March 1999.